Desalination 599 (2025) 118426

Contents lists available at ScienceDirect

Desalination

journal homepage: www.elsevier.com/locate/desal

Hydrate-based desalination process using CO_2 as hydrate forming agent – Modelling and techno-economic analysis

Isabel S. Fernandes [a,b,*], Mariana G. Domingos [c,d], Marcelo F. Costa [c], Ricardo J. Santos [a,b], José Carlos B. Lopes [a,b,d,*]

[a] LSRE-LCM - Laboratory of Separation and Reaction Engineering – Laboratory of Catalysis and Materials, Faculty of Engineering, University of Porto, Rua Dr. Roberto Frias, 4200-465 Porto, Portugal
[b] ALiCE - Associate Laboratory in Chemical Engineering, Faculty of Engineering, University of Porto, Rua Dr. Roberto Frias, 4200-465 Porto, Portugal
[c] CoLAB NET4CO2, Rua Júlio de Matos, 828-882, 4200-355 Porto, Portugal
[d] STAR Institute – Science & Technology Applied Research, Zona Industrial do Salgueiro, Lugar do Pombal, 3530-259 Mangualde, Portugal

HIGHLIGHTS

- Hydrate-based desalination process using CO_2 was modelled in Aspen Plus
- Two cold utilities were considered: heat pump and the heat from LNG regasification
- Hydrate-based process using a heat pump led to an SEC ~ 13.2 kWh·m^{-3}
- Hydrate-based process using LNG cold utility reduces the SEC for 3.8 kWh·m^{-3}
- This desalination technology is a cost-effective solution for water scarcity

GRAPHICAL ABSTRACT

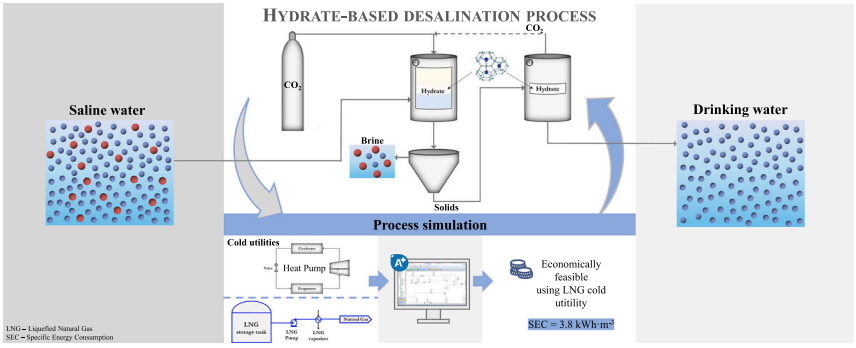

ARTICLE INFO

Keywords:
Desalination
CO_2 hydrates
Process modelling
Economic evaluation
SEC

ABSTRACT

The potential of using CO_2 for hydrate-based desalination is evaluated in this work. CO_2 hydrate formation occurs in a device that uses the NETmix technology and is implemented and modelled in Aspen Plus. To ensure that the vapour-liquid and liquid-liquid equilibria are correctly estimated, the solubility of CO_2 in salt water under incipient hydrate formation conditions is predicted by different property models available in Aspen Plus and compared with published models based on experimental data. The energy and economic costs of the process are then assessed for two process flowsheets, which differ in the cold utility source. In one case, heat pump/refrigeration cycle technology integrates the heat from the hydrate formation and dissociation units, resulting in a Specific Energy Consumption (SEC) within the range of Multi-Stage Flash desalination technologies. In the other case, using the latent heat of natural gas regasification as a cold utility significantly reduced the costs, enabling the production of drinking water with an SEC in the same range as Reverse Osmosis.

* Corresponding authors at: LSRE-LCM - Laboratory of Separation and Reaction Engineering – Laboratory of Catalysis and Materials, Faculty of Engineering, University of Porto, Rua Dr. Roberto Frias, 4200-465 Porto, Portugal.
E-mail addresses: isfernandes@fe.up.pt (I.S. Fernandes), lopes@fe.up.pt (J.C.B. Lopes).

https://doi.org/10.1016/j.desal.2024.118426
Received 23 August 2024; Received in revised form 3 December 2024; Accepted 7 December 2024
Available online 10 December 2024

Nomenclature

$B(T)$	Virial coefficient, [K]
C_{equi}	Equipment cost, [€]
f_{CO_2}	CO_2 fugacity, [bar]
K_0	Solubility constant, [mol·kg^{-1}·atm^{-1}]
M_w	Molecular weight, [kg·mol^{-1}]
n_h	Hydration number
$N_{hours/year}$	Operating hours per year, [h·yr^{-1}]
N_{years}	Economical lifespan, [yr]
p	Pressure, [bar]
p_{eq}	Equilibrium pressure, [bar]
Q_i	Modified Henry's constant, [bar]
r_i	Interest rate
R^2	Coefficient of determination
s	Lattice constant, [m]
S	Salinity
T	Temperature, [°C]
v	Molar volume, [m^3·mol^{-1}]
x_i	Fraction of component i in liquid phase

Greek letters

ΔT_{min}	Minimum temperature approach, [°C]
ρ	Density, [kg·m^{-3}]

Subscripts

A	Avogadro
CO_2	Carbon dioxide
diss	Dissociation
eq	Equilibrium
equi	Equipment
H_2O	Water
h	Hydration
hours/year	Hours per year
L	Liquid phase
min	Minimum
mol	Molar
NaCl	Sodium chloride
years	Years

Acronyms and Abbreviations

APEA	Aspen Process Economic Analyser
ASME	American Society of Mechanical Engineers
BWRS	Benedict-Webb-Rubin-Starling
CAPEX	Capital Expenditures
CEPCI	Chemical Engineering Plant Cost Index
CFD	Computational Fluid Dynamics
COP	Coefficient of Performance
EDR	Exchanger Design and Rating
EoS	Equation of State
HFC	HydroFluoroCarbon
HGtS	Hydrates to transform Gas into Solids
LNG	Liquefied Natural Gas
NIST	National Institute of Standards and Technology
ELECNRTL	Electrolyte Non-Random-Two-Liquid
ENRTL-RK	Electrolyte Non-Random-Two-Liquid-Redlich-Kwong
MED	Multi-Effect Distillation
MSF	Multi-Stage Flash
NG	Natural Gas
OPEX	Operating Expenses
REFPROP	Reference Fluid Properties
REN	Redes Energéticas Nacionais
RO	Reverse Osmosis
R&D	Research and Development
SEC	Specific Energy Consumption

1. Introduction

The increase in the world population and enhanced living standards, accompanied by the expansion of industrial and agricultural activities, led the world demand for fresh water to grow exponentially [1,2]. Moreover, the world's shift from fossil fuels to renewable energy will also add to this rise. Water is the ideal raw material for electrolysis for green hydrogen production [3,4]. Consequently, the supply of readily available fresh water is declining and is becoming scarce. Seawater is the major water source on our planet (97.5 %) [2]; however, it is unfit for human consumption, industrial and agricultural activities, and electrolysis due to the high content of dissolved salts [5]. It is pointed out that about 39 % of the world's population lives at less than 100 km from the sea, thereby desalination is reported as a core technology to generate large amounts of fresh water and, therefore, meet global water supply challenges [6,7].

Desalination is the process of removing dissolved solids, such as salts and minerals, from water [1] using some form of energy. Two streams are generated from desalination: a fresh water stream with a low content of dissolved salts and a concentrated brine stream. The latter is brine rich in raw materials, namely sodium, potassium, magnesium and calcium. Sodium and sodium-ion batteries are pointed as a low-cost energy storage systems [8] to curb the intermittency of renewable energy [9], making desalination play a key role in energy transition.

Desalination technologies can be grouped into thermal processes and membrane-based processes [5]. The first processes proposed for water desalination were the thermal processes, of which Multi-Stage Flash (MSF) and Multi-Effect Distillation (MED) are the most widely used. These processes, however, are being outpaced by membrane-based processes in total desalination capacity, owing to their simplicity, lower energy requirements and cost [10]. Despite these advantages, membrane-based processes still present some limitations. Reverse Osmosis (RO), the leading desalination technology, requires a Total Dissolved Solids (TDS) in feed water lower than 5 %, and has significant fouling. Hydrate-based desalination processes are a promising alternative to overcome this challenge, enabling high concentrations of TDS (~ 30 %) in feed water [7,11].

1.1. Hydrate-based desalination process

Hydrates, also known as clathrates, are solid crystalline compounds resembling ice, composed of cages of hydrogen-bonded water molecules with small non-polar molecules, typically gas molecules, trapped inside [7,12]. Hydrates are formed at low temperatures and high pressure; e.g. CO_2 hydrates require temperatures between 0 and 10 °C and pressures 10 to 60 bar [13].

The clathrate hydrate-based desalination process involves contacting an electrolyte solution (salt water) and a guest compound (hydrate-forming gas) under suitable pressure and temperature conditions, leading to a phase change of water from liquid to solid and the formation of solid hydrates. Because of the salt-removing effect observed in the hydrate formation process, the crystalline structure of the hydrates formed from salt water is free from salts and other impurities, which are concentrated in the liquid phase, without disturbing the morphology of the hydrate crystal [7]. The salt-free hydrates are mechanically separated from the salt-rich liquid phase (e.g. filtration or centrifuge) and then dissociated into fresh water and the guest compound by pressure reduction, heating or both. The hydrate-forming gas can be reused to form new hydrates. Fig. 1 shows a schematic representation of the hydrate-based desalination process.

Compared with freeze distillation, which involves ice crystallisation, hydrate-based processes can operate well above the water freezing point depending on the hydrate-forming gas used. Hence, the refrigeration costs of the process are reduced [14].

The first hydrate-based process was proposed in 1942 [15,16]. The research and development of this technology intensified between the 1960s and 1970s [17]. The main operating issues that prevented the industrialisation of the technology during this period were the difficulty of separating the hydrate crystals and the removal of dissolved hydrate forming agent from the recovered water [17,18]. However,

technological advances have shown that the difficulty of separating the crystals from the brine solution can be surmounted, for example, by using physical processes [7,19].

Knox et al. [20] developed the first desalination plant using propane as hydrate-forming agent. In the mid-1990s, the Bureau of Reclamation commissioned work from Thermal Energy Systems, Inc., to build two pilot plant facilities for seawater desalination in Hawaii and San Diego [21,22]. McCormack [23] describes a clathrate freeze desalination method and apparatus where the hydrate forming agent, HFC R141b, is injected in a submerged pipeline under the sea, where the surrounding temperature is less than the equilibrium temperature for hydrate formation. Then, the hydrate slurry is pumped to the surface.

The hydrate-based process shows to be a promising technology for water desalination. Nevertheless, there are still technical challenges and energy efficiency concerns to overcome that hinder the application at the industrial scale, namely the slow hydrate formation kinetics, a reactor design to enable the production of desalinated water on a large scale and the refrigeration costs [7,24].

The current hydrate-based technologies operate as a batch/semi-batch process [25]. This work proposes, using NETmix technology [26–28], a mesosized static mixer composed of a network of mixing chambers interconnected by transport channels to desalinate water using CO_2 as hydrate-forming gas. This technology was introduced in 2005 at the University of Porto, and pressure drop studies, using Computational Fluid Dynamics (CFD) simulation validated by experiments, showed that pressure requirements for operating NETmix are mainly necessary to promote dynamic mixing. The energy supplied to overcome friction losses is small compared to that dissipated in flow accelerations and decelerations, leading to effective mixing promotion [29]. NETmix was also shown to promote high flow dynamics and interfacial area generation between two immiscible phases [30,31]. This is particularly relevant since mixing CO_2 and water results in a multiphase flow. Besides, it presents heat transfer capacities of $10–10^3$ $MW{\cdot}m^{-3}{\cdot}K^{-1}$, exceeding the typical values for microdevices of 10^{-1}-10^2 $MW{\cdot}m^{-3}{\cdot}K^{-1}$ [32]. A mainly bi-dimensional flow is observed in NETmix due to its planar design. The scale-up of the throughput of this technology can be obtained by numbering up the number of unit cells or combining several NETmix plates in parallel. A unit cell comprises a cylindrical chamber and prismatic half channels oriented at 45° from the main direction. This modular and flexible system makes this technology very versatile and has been experimentally demonstrated for the continuous production of CO_2 hydrate using drinking water [33]. The device used for hydrate formation is a patented modular system [34] composed of a stack of heat exchanger plates coupled to NETmix plates and is known as HGtS - **H**ydrates to transform **G**as into **S**olids. This stack includes a patented closing system [35], which enables enhancing the structural integrity and efficiency of plate reactors. Its convex surface design permits distributing the mechanical stresses evenly along the stack, minimising the likelihood of the impacts of thermal stresses.

The formation of CO_2 hydrates requires low temperature environments (0 to 10 °C). One way to offset refrigeration costs in hydrate-based processes is using the heat absorbed for the gasification of Liquefied Natural Gas (LNG).

1.2. LNG cold utility

The increased environmental concern about air quality and growing demand for clean energy led to Natural Gas (NG) becoming the primary energy resource. In a lot of regions, which do not have their own natural gas resources, natural gas needs to be imported, e.g. all natural gas used in Portugal is either received by a high-pressure pipeline at the Spanish border or by sea in the form of LNG at the Sines regasification terminal [36,37]. The latter is the largest source of NG gas supply in Portugal. LNG presents some advantages over NG, such as being a cleaner fuel due to the removal of most of the impurities of NG during the liquefaction process. Also, the volume reduction makes the transportation of LNG more efficient for long distances than compressed NG in gas pipelines [38]. LNG regasification is pointed out as generating a low amount of greenhouse gas emissions in the context of life cycle assessment [39].

LNG regasification to NG to return to gaseous state is required to transport it to the end user through a pipeline gas network. The LNG is regasified in the terminals by exchanging heat with seawater captured next to the terminal, using open-rack vaporisers. During the regasification of LNG to NG in LNG vaporisers, around 850 $kJ{\cdot}kg^{-1}$ of cold exergy is released into seawater [40]. The latent heat of LNG regasification that is currently wasted can be used for process integration with the hydrate-based desalination process.

He et al. [16] and Chong et al. [14] modelled two hydrate-based processes using Aspen HYSYS software to evaluate the economic viability of the process. The propane was used as a hydrate-forming

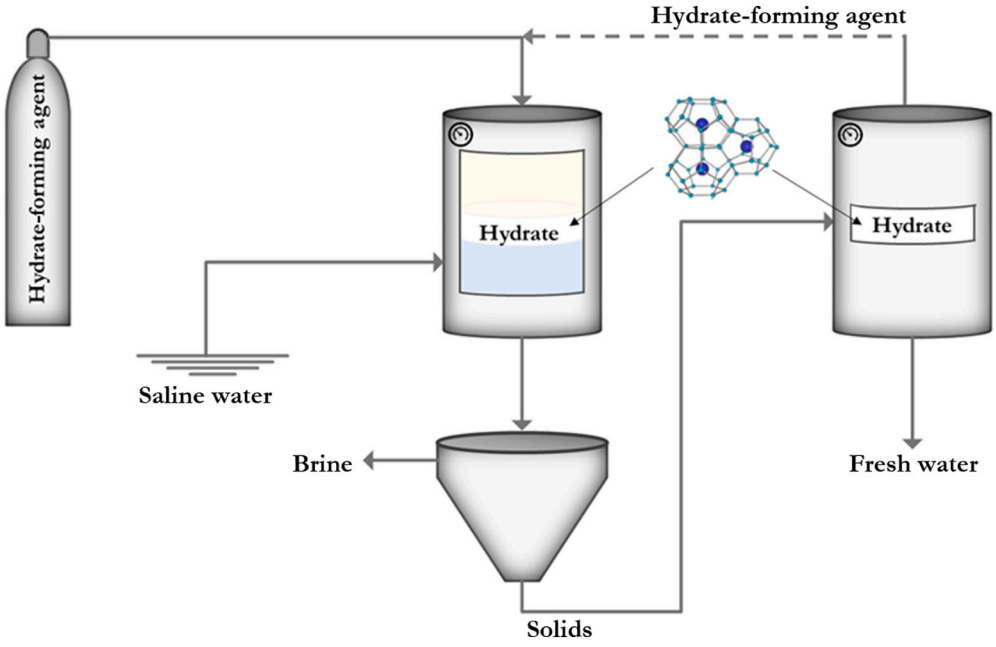

Fig. 1. – Schematic representation of hydrate-based desalination process.

agent and LNG was used as cold energy. The results indicate the hydrate-based process coupled with LNG cold energy utilisation is an attractive option for large-scale applications compared with the leading desalination technologies. Park et al. [41] integrated light hydrocarbon separation and hydrate-based desalination also using propane as the hydrate-forming agent, having shown through process simulation that this process integration leads to a more efficient energy utilisation process than when cold energy is only used for desalination.

This paper presents the modelling of the hydrate-based desalination with NETmix technology using CO_2 as hydrate-forming gas to desalinate seawater in Aspen Plus V12.1. The CO_2 has the advantage, compared with propane, that it is not flammable, and the CO_2 dissolved in recovered water is not harmful. However, propane has more moderate hydrate formation conditions, between 0 °C and 5 °C, the equilibrium pressure to form propane hydrates from fresh water ranges from 1.5 bar to 5 bar, while for CO_2 rises from 12 bar to 23 bar [42]. The fact that CO_2 dissolved in water is not harmful to human consumption is beneficial since it can be sold as sparkling water, which is an extra asset. This also eliminates the need for an additional step to remove the dissolved hydrate-forming agent from water. The separation of CO_2 from flue gas streams from power generation industries combined with fresh water production from salt water is an attractive solution to address both greenhouse gas emissions and water scarcity. The hydrate-based process permits the selective partitioning of the CO_2 component from exhausted gases between the solid hydrate phase and the gas phase through hydrate crystallisation [43,44]. Additionally, Kang et al. [45] showed that the desalting efficiency depends on the hydrate-forming gas and hydraulic pressure, having observed a higher removal efficiency for CO_2 than CH_4. These advantages place CO_2 as a promising hydrate-forming agent for desalination.

Different properties methods were tested to ensure that realistic models were applied to estimate the properties of the components and mixtures. The definition of the hydrate component and the implementation of the unit process where the hydrate formation occurs has already been described in [46], thus, only the changes made will be reported. Two approaches were then adopted regarding the cold utility used. The hydrate-based process was first modelled using ammonia cycles, which were later replaced by LNG cold utility. Ultimately, the potential of hydrate-based processes regarding Specific Energy Consumption (SEC) is compared with leading desalination technologies.

2. Model implementation

An accurate estimation of vapour-liquid and liquid-liquid equilibrium, particularly the ternary mixture [CO_2-H_2O-NaCl], is essential to model the system. Other salts present in seawater were not considered in this work. Although NaCl accounts for over 85 % of TDS in typical seawater composition, recent studies indicate that some of the other salts present, e.g. $MgCl_2$, significantly influence the formation rate and the stability of CO_2 hydrates [47], and are removed via hydrate formation, e.g. Na^+, K^+, Mg^{2+}, $Ca^{2+}$and B^{3+} cations and Cl^- and SO_4^{2-} anions [45,47]. Also, other promoters can be added to improve the CO_2 gas uptake and lower the incipient hydrate formation conditions [48,49]. Montazeri et al. [50] investigated the use of CO_2 nanobubbles as a kinetic promoter for hydrate-based desalination for 0.5 M NaCl and synthesised seawater solution, prepared by dissolving NaCl, KCl, $MgCl_2$, $MgSO_4$ and $CaCl_2$ in appropriate amounts. They observed an 86 % reduction in induction time due to the presence of CO_2 nanobubbles and ions removal efficiencies of 41.3 % for the 0.5 M NaCl solution and between 40 % and 50 % for the synthesised seawater. Since sodium chloride is the predominant salt in seawater and there is a more extensive wealth of knowledge in the literature on CO_2 formation in NaCl solutions, the effects of other ions in seawater were not considered in process simulation. However, the methodology developed to create an automated framework for simulating the hydrate-based desalination process can be easily adapted once comprehensive thermodynamic data on the salty solution, incorporating all the salts, becomes available.

Two necessary thermodynamic conditions are required for hydrate formation: the temperature and pressure conditions within the hydrate stability region (equilibrium conditions), and a supersaturated environment, i.e., the amount of guest molecule in the system must be larger than the solubility of the gas in water.

The first step involved analysing the incipient hydrate formation conditions, i.e. conditions above which hydrate formation takes place. Sun et al. [51], Mohammadi et al. [52], and Dholabhai et al. [53] reported some data on the hydrate phase equilibrium of CO_2 in the presence of various concentrations of NaCl solutions. Fig. 2 compares the CO_2 hydrate equilibrium curves obtained in the CSMGem (Colorado School of Mines – Gibbs energy minimisation) software with the experimental data reported by these authors. CSMGem was developed by Ballard [54] and enables the prediction of the multiphase equilibrium at any given pressure, temperature and composition through the minimisation of Gibbs energy [12].

For reference, a typical seawater salt content of 3.5 % (m/m) NaCl was also shown (dashed line).

The salt acts as a thermodynamic inhibitor, reducing the driving force for hydrate formation and, therefore, retarding the growth of hydrate crystals [7,19]. For this reason, as observed in Fig. 2, an increase in salt fraction shifts the incipient hydrate curve to lower temperatures and larger pressures. The data presented by the authors agree with the forecast obtained from CSMGem, and the increase in the equilibrium pressure at the same temperature is more pronounced for higher temperatures, noticing an approximation between the curves as the temperature approaches 0 °C. This indicates that the operating costs related to the compression and refrigeration of feed streams of the hydrate-based desalination process increase with the salinity of the feed water.

The next step was the estimation of CO_2 solubility in seawater, considering the hydrate formation conditions given by the CSMGem software. The carbon dioxide solubility was analysed under the temperature and pressure conditions of the grey dashed line shown in Fig. 2, and a temperature range between 0 and 8 °C, since these temperatures correspond to the lower and upper quadruple points, respectively, of the CO_2-seawater system. The quadruple points identify the four-phase coexistence, the equilibrium between ice-liquid salt water-hydrate-gaseous CO_2 and liquid salt water-hydrate-gaseous CO_2-liquid CO_2.

The solubility was estimated using CSMGem, Aspen Plus (with various electrolytic models and the Henry's law for modelling the salt and the CO_2 in liquid solution), and the model developed by Weiss [56]. The latter was based on independent measurements of Li et al. [57] and Murray et al. [58], after correcting it to consider the non-ideal behaviour of CO_2 in the gas phase and the dissociation of dissolved hydrated CO_2 to form bicarbonate - see supplementary material.

Aspen Plus, electrolyte activity coefficient models were selected because of the presence of the salt, as charged species make the electrolytic systems strongly non-ideal.

The analysis of Fig. 3 shows that the thermodynamic models Electrolyte Non-Random-Two-Liquid (ELECNRTL), symmetric and unsymmetrical Electrolyte Non-Random-Two-Liquid-Redlich-Kwong (ENRTL-SK and ENRTL-RK, respectively) provide a good representation of the calculation of the CO_2 solubility from the equations proposed by Weiss [56]. ENRTL-RK and ENRTL-SR use the ELECNRTL model with two different Equation of State equations: Redlich-Kwong (RK) and Soave-Redlich-Kwong (SRK). The use of these EoS for modelling the gas phase was shown to increase the accuracy of CO_2 solubility in water, permitting considering the vapour-liquid equilibrium and ion formation. PITZER methods are appropriated for highly concentrated solutions, accounting for long-range electrostatic interactions [59]. Thus, this model diverges from Weiss's prediction as low concentrations are associated with CO_2 dissolution in water, overestimating the CO_2 solubility values. ENRTL-HF and ENRTL-HG are modifications of the ELECNRTL model; the first was designed particularly for hexamerization using

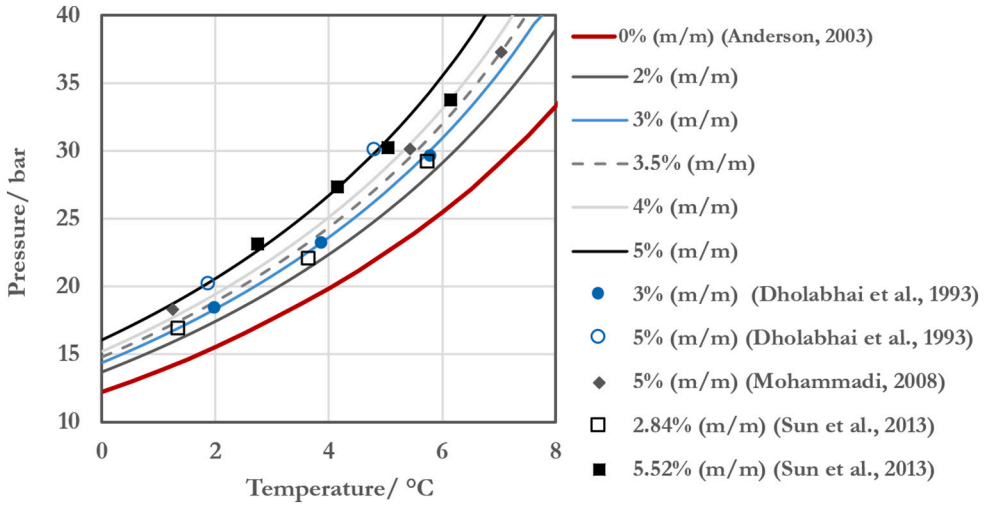

Fig. 2. CO_2 hydrate equilibrium curve for various concentrations of NaCl solutions. Lines represent data extracted from CSMGem. The points correspond to experimental data retrieved from Sun et al. [51], Mohammadi et al. [52], and Dholabhai et al. [53]. For unsalty water, the equation proposed by Anderson [55] was used.

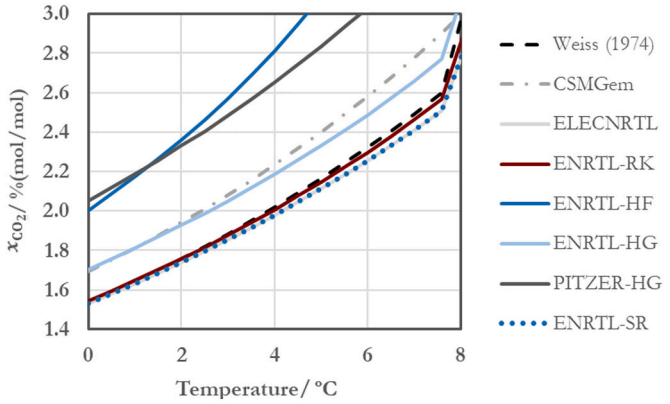

Fig. 3. CO_2 solubility in seawater (3.5 % NaCl (m/m)) under CO_2 hydrate equilibrium curve.

hydrogen Fluoride (HF) association for the vapour phase model, and the second uses the Helgeson model for standard properties calculations. Still, the deviation observed shows that they don't accurately capture the hydrogen bonding between water and dissolved CO_2. Moreover, it is observed that the CO_2 solubility values retrieved from CSMGem are considerably higher at the same temperature than those predicted by Weiss [56]. As ENRTL-RK is the thermodynamic model that gives a closer prediction of the values obtained through the equations proposed by Weiss [56], it was chosen as the global property method for the process simulation of the hydrate-based desalination plant.

Aspen Plus User-2 block was used to represent the HGtS, the process unit where salt is separated from water through hydrate formation. The User-2 block is a customised block that enables the communication between Aspen Plus and an Excel workbook. Aspen Plus writes the input data in Excel, then the calculation is performed in the workbook, and next, it reads back the output data. Thus, the equations needed to estimate the HGtS outlet composition and the enthalpy of hydrates formed were added to an Excel worksheet. An algorithm was developed to estimate the hydrate formation in the presence of NaCl solutions, as shown in Fig. 4.

The first step carried out by the block is to verify that the conditions for the formation of hydrates are met. The equilibrium curve for a mass percentage of NaCl of 3.5 %, given by CSMGem (Fig. 2) was fitted to a 4th-degree polynomial

$$p_{eq}\Big/\,\text{bar} = 2.77\times10^{-3}(T/\,^{\circ}\text{C})^4 - 1.81\times10^{-2}(T/\,^{\circ}\text{C})^3 + 2.06 \times 10^{-1}(T/\,^{\circ}\text{C})^2 + 1.66\left(T\Big/\,^{\circ}\text{C}\right) + 14.8 \quad (1)$$

which is valid between 0 and 8 °C.

The block calculates the equilibrium pressure using Eq. 1 for the operating temperature of HGtS and compares it with the operating pressure. If the operating pressure is lower than the equilibrium pressure no hydrate formation occurs, and the outlet composition corresponds to the mixing of inlet streams; if it is higher, then supersaturated condition is evaluated.

For that purpose, the equations proposed by Weiss [56] and described in the supplementary material were introduced in the block to estimate the solubility of CO_2 in seawater at operating temperature and the corresponding equilibrium pressure. Hydrate formation occurs if the amount of CO_2 in the feed streams exceeds solubility.

The mass balance in the presence of hydrates is calculated following the approach described in [46] and Fig. 4, for CO_2 from unsalted water, since the salt is not enclatherated in the water cavities of the CO_2 hydrate structure. The salt in feed water leaves at the outlet liquid phase of HGtS, so it is not considered in the equations that describe the formation of CO_2 hydrates.

The hydration number for the equilibrium conditions of the CO_2 hydrate formation curve for a 3.5 % NaCl (m/m) solution was estimated from the following equation, obtained from data from CSMGem, and valid in the temperature range of 0 to 8 °C

$$n_h = 6.33\times10^{-4}(T/\,^{\circ}\text{C})^2 - 4.86\times10^{-2}(T/\,^{\circ}\text{C}) + 6.68 \quad (2)$$

The hydration number at 3 °C, obtained using Eq. 2, is 6.5. This value aligns with the data from different authors for CO_2 hydrate formation in pure water, which range from 6.2 to 6.5 [55,60–62].

The procedure for estimating the enthalpy of dissociation of solid hydrate formed in pure water described in [46] was followed to determine hydrate dissociation of hydrates formed in saline water. However, the molar volume of the liquid phase now accounts for the contribution of NaCl in addition to the CO_2 and water. The expression used for v^L calculation was proposed by Duan et al. [63] - see supplementary material Eq. B.1. The density of CO_2 hydrates was determined using the equation proposed by Teng et al. [64]. These equations were introduced in HGtS block (User-2). Fig. 5 systematises the algorithm developed to solve the energy balances for hydrate formation.

The enthalpy of hydrate dissociation was determined using the Cla-

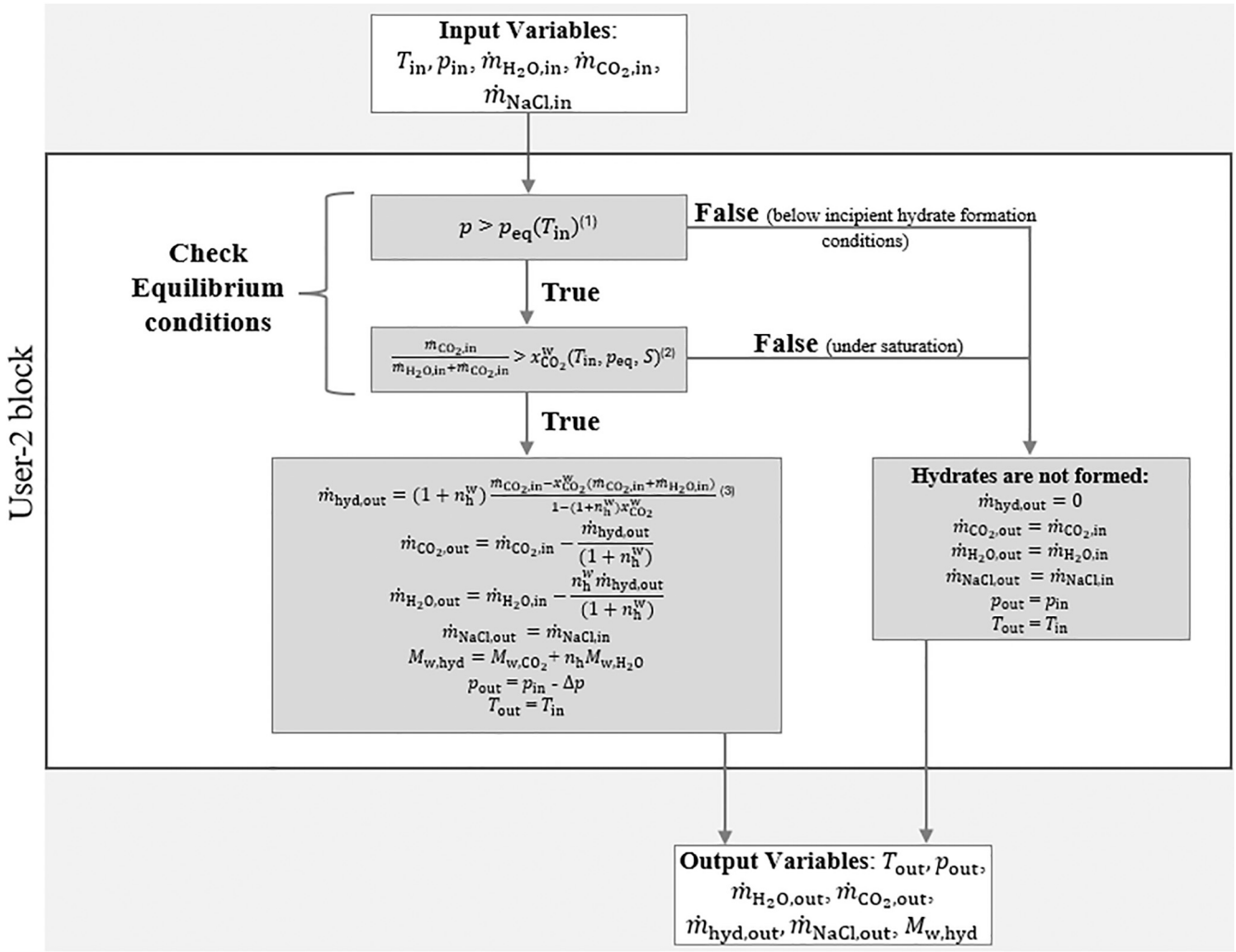

$\dot{m}_i$ - mass flow rate of species i = H_2O, CO_2, NaCl and hyd
$M_{w,i}$ - molecular weight of species i = H_2O, CO_2, NaCl and hyd
p - pressure
Δp - pressure drop
S - salinity
T - temperature
out - outlet
in - inlet
(1) $p_{eq}(T_{in})$ - Eq. (1)
(2) $x^w_{CO_2}$ - solubility estimated by Weiss [56]
(3) $n^w_h = n_h \frac{M_{w,H_2O}}{M_{w,CO_2}}$, n_h - hydration number - Eq. (2)

Fig. 4. – User-2 algorithm for solving the mass balances in HGtS.

peyron equation. For a temperature of 3 °C, T_{in}, this value was estimated to be 57.1 kJ·mol^{-1}.

Additionally, to run a simulation with the hydrate presence, the density, molar weight, specific heat capacity, and hydrate formation enthalpy at 25 °C of CO_2 hydrates have to be introduced in the component's specifications tab of the Aspen Plus property environment.

3. Case 1: Refrigeration cycle as cold utility hydrate-based desalination flowsheet

3.1. Process description

The Aspen Plus V12.1 flowsheet for seawater desalination through continuous formation of CO_2 hydrates is shown in Fig. 6. The global property method of the hydrate-based desalination process was ENRTL-RK. In the lines where only CO_2 is present, the process units were modelled with Peng-Robinson and refrigeration cycles/heat pump with Reference Fluid Properties (REFPROP). ENRTL-RK is an activity coefficient method, thus, it is more suitable for accurate liquid-phase interactions and for systems up to moderate pressures for which the vapour-phase non-ideality is small. Therefore, Equation of State (EoS) methods were applied for CO_2-only lines and modelling of refrigeration cycles and heat pumps. Peng-Robinson is particularly suitable for hydrocarbons and light gases like carbon dioxide. REFPROP was developed by the National Institute of Standards and Technology (NIST). This model is particularly appropriate for estimating the thermodynamic and transport properties of natural gas systems and their mixtures of refrigerants and hydrocarbons [65].

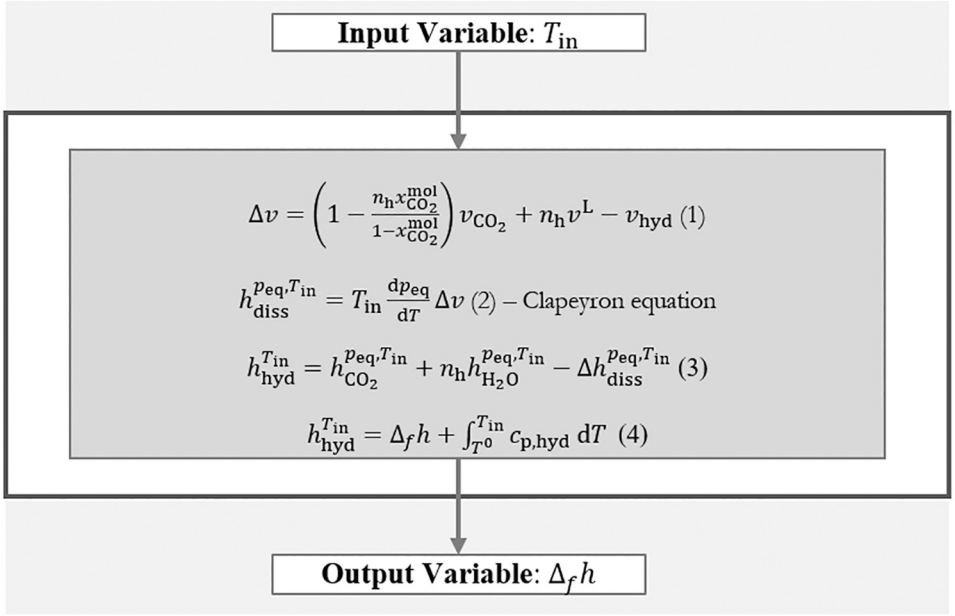

(1) Δv - specific molar volume change – Anderson [55]
n_h - hydration number - Eq. (2)
$x_{CO_2}^{mol}$ - molar solubility estimated by Weiss [56]
$v_{CO_2} = \frac{M_{w,CO_2}}{\rho_{CO_2}}$, v_{CO_2} - CO_2 molar volume, ρ_{CO_2} - CO_2 density estimated from NIST database Eq. (B.3)
v^L - molar volume of the liquid phase - Eq. (B.1)
v_{hyd} - Teng et al. [64]
(2) $h_{diss}^{p_{eq},T_{in}}$ - enthalpy of hydrate dissociation
p_{eq} - equilibrium pressure - Eq. (1)
(3) $h_{hyd}^{T_{in}}$ - solid enthalpy of formation at T_{in}
$h_{CO_2}^{p_{eq},T}$ – molar enthalpy of CO_2 ~ 395 kJ·mol^{-1}
$h_{H_2O}^{p_{eq},T}$ - molar enthalpy of CO_2-saturated water ~ 290 kJ·mol^{-1}
(4) $\Delta_f h$ - solid enthalpy of formation at T^0 - reference temperature - 25 °C and 1 atm
$c_{p,hyd}\ (kJ \cdot kg^{-1} \cdot K^{-1}) = 2.12 \times 10^{-1} + 6.98 \times 10^{-3}(T(°C) + 273.15) - 4.81\ (T(°C) + 273.15)^{-1}$ - hydrate specific heat

Fig. 5. – User-2 algorithm for solving the energy balances in HGtS.

3.1.1. Hydrate formation

The HGtS (**R-1**), modelled using the User-2 block, described in Section 2, operates isothermally at 3 °C and 27 bar with a pressure drop of 3 bar. The equilibrium pressure for CO_2 hydrates formation at 3 °C is 21.3 bar; thus, it is guaranteed that the inlet and outlet pressure of HGtS is larger than the equilibrium pressure. The hydrate formation rate is not modelled within **R-1**, as previous studies have demonstrated that the NETmix technology is capable of producing a hydrate slurry at a space-time yield of 200 t·h^{-1} m^{-3} [33]. Heat integration was done to minimise the demand for cold and hot utilities. The heat duty in heat exchangers is presented in bold next to these equipment.

The seawater inlet stream is fed at 1 bar and 10 °C, and is then pressurised to 27.5 bar using pump **P-2**, and cooled to 3 °C (**E-2** and **E-3**). The NaCl mass percentage in saline water is 3.5 % (m/m). For the cooling to 3 °C, the stream is divided into two branches. One exchanges heat with the CO_2 makeup stream and the other with a refrigeration cycle.

The inlet conditions of CO_2 are typical of CO_2 storage in tanks (−40 °C and 22 bar (ASCO carbon dioxide Ltd. [66])). In this case study, the amount of CO_2 fed to HGtS was fixed at 10 t·h^{-1}, and the mass flow rate of water was determined, resorting to a design-spec block, to obtain a CO_2 hydrate slurry at the reactor outlet with a mass percentage of solids of 20 % in agreement with [33]. This percentage ensures a significant amount of water in excess, to enable the formation of the solid particles in a slurry that is diluted enough to avoid plugging. The amount of CO_2 fed to the HGtS is 10 t·h^{-1}, but nearly half is recirculated. A CO_2 makeup with a mass flow rate of 4.7 t·h^{-1} is used to suppress the CO_2 that exits the process dissolved in water in the brine and fresh water streams. At inlet conditions, the CO_2 is in the liquid state, so it is pressurised using pump **P-1** to 27 bar and then is heated by exchanging heat in **E-1** with the fresh water stream required for washing the surface of the hydrates, which needs to be cooled, and with the saline water in the heat exchanger **E-2**. The CO_2 makeup stream is mixed with the CO_2 recycling stream and is fed to the HGtS.

3.1.2. Preparation of hydrate slurry and dissociation

The CO_2 hydrates formed are free from salt, however, it is reported that some salt stays entrapped in interstitial spaces of the hydrate. A hydrocyclone (**S-1**) and a wash column (**S-2**) were modelled to overcome this issue. At the solid-liquid separator **S-1** exit, the hydrate lattice presents a mass percentage of solids of 90 %, and the other stream is a brine solution with 4.0 % NaCl (m/m). The hydrate lattice enters the wash column, where it contacts with CO_2-saturated water to remove any adhering salt from the surface of the hydrates.

The fresh water and CO_2 streams modelled to produce the CO_2-saturated water to feed the wash column can be replaced by providing

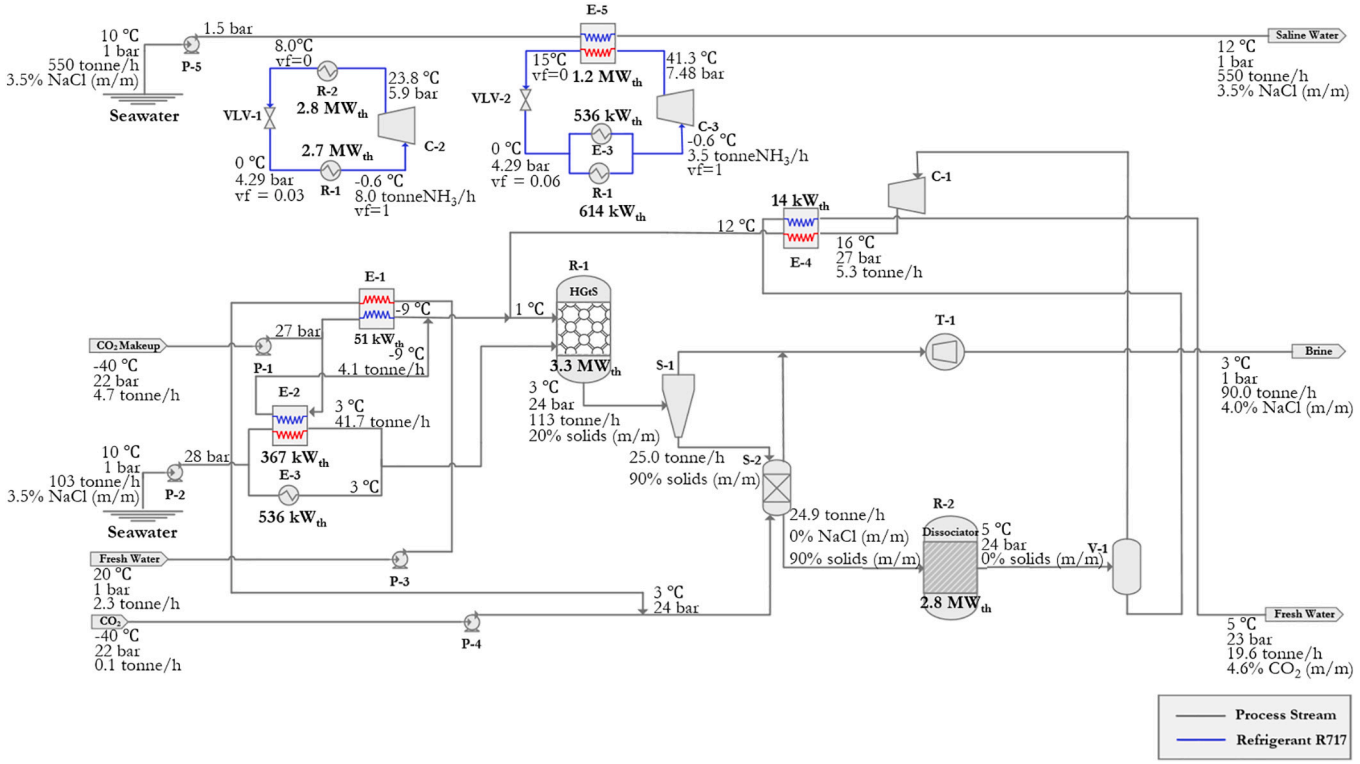

Fig. 6. – Process diagram of the facility for seawater desalination through CO_2 hydrates production, where *C* stands for compressor, *E* for heat exchanger, *P* for pump, *R* for reactor, *T* for turbine, *V* for flash vessel, *S* for separator, *VLV* for valve and *vf* for the vapour fraction.

part of the fresh water flow produced in the process, being necessary to cool this stream from 5 °C to 3 °C. As the solubility in CO_2 increases with decreasing temperature, mixing some CO_2 to saturate the stream under conditions of 3 °C and 23 bar would be required.

After passing the washing column (**S-2**), the liquid phase of the hydrate lattice is free from salts, maintaining the liquid fraction of the hydrate lattice practically unchanged, with a mass percentage of solids of 90 % that proceeds to the dissociator (**R-2**). The mass flow rate of CO_2-saturated water fed to the washing column is the same as the liquid phase in the hydrate lattice at the **S-1** outlet. Thus, the amount of fresh water to produce this CO_2-saturated water stream was fixed at 2.3 $t{\cdot}h^{-1}$ and the temperature and pressure at 20 °C and 1 bar, respectively. This stream was pressurised using pump **P-3** and cooled in heat exchanger **E-1** to the outlet operating conditions of the HGtS reactor (3 °C and 24 bar). The amount of CO_2 needed to saturate the fresh water stream at 3 °C and 24 bar was estimated as 0.1 $t{\cdot}h^{-1}$. The inlet conditions are the same as the CO_2 makeup stream; pump (**P-4**) was used to set the operating pressure to 24 bar. Then, the fresh water and CO_2 are mixed and fed to the wash column. A hydrate lattice without salt is obtained from the wash column, and the saline solution is mixed with the saline solution that leaves the hydrocyclone **S-1**. This stream passes through a hydroturbine (**T-1**) that permits energy recovery by depressurising the liquid stream to 1 bar. The hydrate lattice goes to the dissociator (**R-2**), where the hydrates are disintegrated through heat stimulation ($CO_2{\cdot}n_hH_2O$ (hydrate) → CO_2 + n_hH_2O, in this case, the hydration number at 3 °C is 6.5). The hydrate stream is heated up to 5.0 °C, and the dissociation heat is provided in this unit. The equilibrium pressure for hydrate formation is around 28 bar for this temperature, so hydrates are unstable. It is assumed that the rate of hydrate dissociation is larger than the feed rate, which is reasonable considering that the heat transfer rates of the micro/mesoreactors used are considerably larger than conventional reactors [32]. The CO_2 hydrates are dissociated in a two-phase liquid mixture composed of CO_2-saturated water free from salt and CO_2 in the gaseous state. This mixture goes to a flash unit (**V-1**) to separate the gas and liquid phases. The liquid phase, composed of water saturated in CO_2, exchanges heat in **E-4** and is the fresh water stream produced in the process. This fresh water stream is carbonated water and leaves the process at 23 bar.

3.1.3. *Fresh water stream and CO_2 makeup*

The fresh water stream produced can be sold as a carbonated drink. CO_2 is an inert, non-toxic gas, practically tasteless [67]. The amount of CO_2 in the liquid phase of fresh water stream is 45 $g{\cdot}l^{-1}$. The CO_2 impregnation to produce carbonated drinks can occur naturally or by an artificial process and typically involves cold CO_2 under higher pressure [68]. The temperature and pressure temperatures depend on the method used and the desired level of carbonation. A typical carbonated soft drink contains between 6 and 8 g of CO_2 per litre [69]. So, if the pressure of the produced fresh water stream is reduced, for example, to 2 bar, the amount of CO_2 in the liquid phase is around 6.4 $g{\cdot}l^{-1}$, which is in the range of typical values for drinking sparkling water. The CO_2 that is no longer dissolved in the liquid phase can be reused in the hydrate formation process, reducing the mass flow rate of the CO_2 makeup stream. If it is intended to produce still water, i.e., water without or with a small amount of dissolved CO_2, degasification methods to remove the dissolved CO_2 should be considered, such as aeration, [70], heating [71], membrane degasification [72], and chemical precipitation [73].

The gaseous stream that leaves the flash unit is essentially composed of CO_2 (99.98 % of CO_2 on a mass basis, being the remaining water). This stream is compressed in compressor **C-1** to suppress the pressure drops in the process and is cooled to 12 °C by exchanging heat in **E-4** with the fresh water produced in the process. Then, it is reused to form new hydrates.

3.1.4. *Refrigeration cycles*

Two refrigeration cycles were modelled, both using ammonia as a refrigerant. One permits removing the heat from the HGtS (**R-1**) required to ensure the isothermal operation at 3 °C and supplies the heat

necessary to hydrate dissociation in the dissociator (**R-2**). This ammonia cycle can be seen as a refrigeration cycle or heat pump, as the system permits the cooling of the HGtS fluids through the evaporation of the refrigerant (acting as a refrigeration cycle) and the heating of the dissociator fluids through the condensation of the refrigerant (acting as a heat pump). In this refrigeration cycle/heat pump represented in the upper LHS of Fig. 6, ammonia circulates in a closed loop. Ammonia circulates in the heat exchanger plates of HGtS, which evaporates and removes the heat generated in the reactor. The dissociator was modelled as a heat exchanger where the heat that needs to be supplied for hydrate dissociation is obtained through the condensation of ammonia. The ammonia stream is fed on the hot side of the dissociator, and on the cold side the CO_2 hydrates. The circuit modelled permits removing 2.7 MW_{th} from the HGtS. The Coefficient of Performance (COP) in terms of cooling of this refrigeration cycle is 24.4. Another refrigeration cycle was modelled to remove the remaining heat from HGtS and cool part of the inlet seawater stream (60.8 $t{\cdot}h^{-1}$). In this case, saline water as a cold utility is applied to obtain the condensation of ammonia in the heat exchanger **E-5**, which results in a weaker performance of this refrigeration cycle as the evaporator temperature is the same (0 °C) as it is needed to cool the streams to 3 °C and the condensing temperature is now higher 15 °C. The COP of this refrigeration cycle is 13.9.

3.2. Equipment design specifications and economic evaluation

The pressure drop in heat exchangers due to friction was modelled using conservative values [74,75]. For vapour, liquid, condensing and boiling streams, the values considered were 0.15, 0.5, 0.2, and 0.1 bar, respectively.

The heat exchangers that exchange heat between process streams were modelled with a minimum temperature difference, ΔT_{min}, of 5 °C. A minimum temperature difference of 3 °C was used in refrigeration cycles except for the saline water cooler **E-5**, where $\Delta T_{min} = 5$ °C was chosen. The outlet temperature of the hot stream of **E-4** (compressed CO_2) was defined as 12 °C, corresponding to $\Delta T_{min} = 7$ °C, which intends to prevent negative CO_2 temperatures at the inlet of the HGtS, which could lead to water freezing. A minimum temperature difference of 3 °C was considered for heat exchangers where refrigerant is used and 5 °C for water coolers, considering that it is possible to operate plate heat exchangers in counter-flow as low as 2 °C [76].

Regarding the design conditions of the refrigeration cycle/heat pump which absorbs most of the heat from the HGtS (**R-1**) and provides the heat to the dissociator (**R-2**), the heat of the ammonia condenser (**R-2**) was fixed at the value of heat duty of reactor **R-2** (2.8 MW_{th}), this enabled the determination of the ammonia flow rate needed in the circuit (8.0 $t\ NH_3{\cdot}h^{-1}$).

The dissociator receives heat from the ammonia condensation in the refrigeration cycle/heat pump. In this ammonia condenser, the outlet vapour fraction is set to 0, and the outlet temperature to 8 °C. This temperature was defined considering $\Delta T_{min} = 3$ °C regarding the dissociator (**R-2**) outlet stream temperature (5 °C). Although the ammonia flows in counter current with the hydrates in the dissociator, the temperature gap was established based on the two outlet streams because ammonia condensation occurs around 8 °C; thus, most of the heat released by ammonia is at this temperature. The outlet pressure of valve **VLV-1** was set so that the ammonia inlet temperature in the evaporator (**R-1**) is 0 °C. For modelling the ammonia evaporation in heat exchanger plates of HGtS, the outlet vapour fraction of ammonia was fixed at 1, and the compressor **C-2** discharge pressure was determined by defining the outlet temperature of the ammonia in **R-2** (8 °C).

A similar approach was adopted for design the other refrigeration cycle, which removes 614 kW_{th} from the HGtS and cools the saline water (536 kW_{th}) fed to the HGtS. The ammonia temperature at the outlet of the condenser (**E-5**) is higher for this refrigeration cycle, which increases the discharge pressure of compressor **C-3**. After ammonia passes through valve **VLV-2**, the total flow is divided into two branches: one exchanges heat with HGtS and the other with saline water in **E-3**. The ammonia flow rate in each branch, which is proportional to the heat removed, is 1.86 $t\ NH_3{\cdot}h^{-1}$ for the HGtS (**R-1**) and 1.62 $t\ NH_3{\cdot}h^{-1}$ for the seawater (**E-3**). The seawater used as a cold utility in **E-5** enters at 10 °C and 1 bar, and is pressurised to 1.5 bar using **P-5** to compensate for the pressure drop in the heat exchanger. The outlet temperature of saline water was defined to avoid a temperature cross-over of cold and hot streams in **E-5**. The ammonia condensation occurs at around 15 °C, thus the outlet stream of saline water was set at 12 °C, resulting in a mass flow rate of saline water 550 $t{\cdot}h^{-1}$. The condensing temperature was defined considering $\Delta T_{min} = 5$ °C concerning the inlet temperature of saline water in **E-5**, which was specified as 10 °C.

All the pumps were modelled with an efficiency of 80 %, and the compressors and turbine with 90 %.

The design, rating and cost estimation of the heat exchangers was done using the Exchanger Design and Rating (EDR) package. The selection of equipment type and capital cost estimation of the other equipment was done using APEA software. The costs retrieved from APEA include material and manpower costs. All the equipment costs are related to the pricing basis for the 1st quarter of 2019 and were obtained using Europe as the project region. The cost of the HGtS reactor was estimated considering the guidelines provided by CoLAB NET4CO2, which are exploiting this technology into industrial projects.

The equipment cost of the hydrate-based desalination process is shown in Table 1.

The total equipment was estimated to be 4.3 M€. 47 % of the total cost is allocated to the compressors of refrigeration cycles. The cost from 2019 was adjusted to 2023 using Chemical Engineering Plant Cost Index (CEPCI):

$$C_{equi}(2023€) = C_{equi}(2019€)\frac{(CEPCI(2023))}{(CEPCI(2019))} \tag{3}$$

where CEPCI (2023) and CEPCI(2019) are 800.8 and 607.5, respectively. The $C_{equi}(2023€)$ were estimated at 5.66 M€.

The Capital Expenditure (CAPEX) cost was calculated normalising the equipment costs, C_{equi}, by the process productivity for fresh water (FW), $\dot{P}_{FW}$, using the following expression.

$$CAPEX = \frac{\sum_i C_{equi,i}(2023€)}{N_{hours/year}\dot{P}_{FW}}\frac{(1+r_i)^{N_{years}}}{N_{years}} \tag{4}$$

where r_i is the interest rate, $N_{hours/year}$ is the operating hours per year,

Table 1
– Equipment cost of the hydrate-based desalination process.

	Total Cost/k€
CO_2 makeup pump (**P-1**)	34.9
Saline water pump (**P-2**)	249
Fresh water pump (**P-3**)	23.9
CO_2 pump (**P-4**)	19.3
Saline water pump (**P-5**)	228
CO_2/Fresh water heat exchanger (**E-1**)	0.78
CO_2/Saline water heat exchanger (**E-2**)	2.60
Saline water heat exchanger (**E-3**)	9.55
CO_2/Fresh water heat exchanger (**E-4**)	0.76
Brine turbine (**T-1**)	48.8
CO_2 compressor (**C-1**)	533
HGtS (**R-1**)	403
Dissociator (**R-2**)	356
Hydrocyclone (**S-1**)	98.2
Gas-Liquid separator (**V-1**)	146
Refrigeration cycle/Heat pump	
Ammonia condenser (**E-5**)	127
Ammonia compressor (**C-2**)	1000
Ammonia compressor (**C-3**)	1011
Total	4292

and N_{years} is the economic lifespan. The interest rate was considered 0 due to increased public financing for supporting desalination technologies, $r_i = 0$. Several funding mechanisms for Research and Development (R&D) and demonstration projects have been established through research framework programs and other EU funding sources [77]. For a reference interest rate of 4.5 %, the CAPEX increases by 200 % in both cases, which results in an 84 % increase in the total cost for the pumped/refrigeration case and a 119 % increase for the LNG case. Nevertheless, the LNG will always remain the least expensive option. The $\dot{P}_{FW}$ obtained from the main simulation was 19.6 $t{\cdot}h^{-1}$; a 2-week break per year was assumed resulting in $N_{hours/year}$ 8400 $h{\cdot}yr^{-1}$ and N_{years} equal to 25 yr was considered, which is the a typical life span for desalination plant [78]. This resulted in a CAPEX cost of 1.38 €·(tonne FW)$^{-1}$.

The operating costs were directly proportional to the electrical consumption of the equipment, as electricity is the only utility needed for the process. Table 2 shows the electrical power per process unit. No cost has been attributed to saline water, CO_2, or unsalted water consumed in the process, nor to the NH_3 load required in the refrigeration cycle or to compensate for losses in closed circuits, as this was considered negligible relative to electricity. The temperature of seawater streams fed to the process was considered 10 °C (Section 3.1). Water temperature in the Atlantic Ocean in Sines ranges from 17 °C to 20 °C. However, the water temperature for extraction offshore at depths below 200 m is 4 °C. The CAPEX for this water source is not considered in the economic assessment. Furthermore, the cold utility in this case study is not a limiting factor. Currently, the open-rack vaporisers for LNG regasification at Sines refinery are already producing a seawater waste stream, so water availability at 10 °C is considered a conservative approach.

The electrical power requirement is 260 kW_e, which results in a cost of 37.6 €·h^{-1} considering a unit cost for electricity of 0.1446 €·kWh^{-1}. This was the electricity price for non-household consumers in Portugal in 2023, provided by Eurostat [79].

The OPEX cost was calculated by dividing the cost per hour by the productivity, resulting in 1.92 €·(tonne FW)$^{-1}$. It should be noted that the refrigeration cycles modelled in the process (**C-2** and **C-3**) represent 75 % of the total electrical consumption of the process. The Specific Energy Consumption (SEC), defined as the ratio of the total energy consumption to the volumetric flow rate of fresh water, is 13.2 $kWh{\cdot}m^{-3}$. The SEC of RO and MSF for seawater treatment is reported as 3–4 $kWh{\cdot}m^{-3}$ and 10–16 $kWh{\cdot}m^{3}$, respectively [14]. The hydrate-based technology employing ammonia cycles falls within the SEC range stated for MSF.

The total cost of producing fresh water using a hydrate-based desalination process, i.e., the sum of OPEX and CAPEX costs, is 3.29 €·(tonne FW)$^{-1}$.

The analysis of the costs shows that the main cost of desalination through the formation of CO_2 hydrates is associated with the equipment cost of the refrigeration cycles/heat pump compressors and the electricity costs associated with them. The following section evaluates the possibility of energy integration of the latent heat of Liquified Natural Gas (LNG) regasification, typically done in coastal areas [41], with the hydrate-based desalination process to offset the refrigeration requirements.

Table 2
– Electrical power in the hydrate-based desalination process.

	Electrical Power/ kW_e
CO_2 makeup pump (**P-1**)	0.66
Saline water pump (**P-2**)	93
Fresh water pump (**P-3**)	1.9
CO_2 pump (**P-4**)	6.5×10^{-3}
Saline water pump (**P-5**)	9.4
Brine turbine (**T-1**)	−50
CO_2 compressor (**C-1**)	11
Ammonia compressor (**C-2**)	111
Ammonia compressor (**C-3**)	83
Total	260

4. Case 2: LNG as cold utility

4.1. Process description

Near the Sines terminal, several chemical industries, such as GALP Energia and Repsol Polímeros, emit CO_2. This presents an opportunity to utilise CO_2 sources directly in hydrate-based processes. A future study will explore the use of a hydrate-based method for CO_2 separation from flue gas. Therefore, the location of the LNG regasification terminal in Sines is well-suited for implementing a hydrate-based desalination process that uses CO_2 as a hydrate-forming agent.

An LNG with 99.34 % CH_4 (mol/mol), 0.51 % C_2H_6 (mol/mol), and 0.15 % N_2 (mol/mol), at −162 °C and 85 bar was considered. This inlet temperature was based on [14] and the inlet pressure was based on the target pressure of the high-pressure pumps in the terminal of Sines that pressurise the LNG prior to vaporisation, as indicated by Redes Energéticas Nacionais (REN) - the Portuguese company that works on the transport of high-pressure natural gas [36]. Any heating caused by the pressurisation to 85 bar is neglected. The LNG/NG lines were modelled using the BWRS property method, based on the Benedict-Webb-Rubin-Starling EoS, which is particularly suitable for natural gas mixtures [65].

The process flow diagram of hydrate-based technology using LNG as cold utility is shown in Fig. 7.

The LNG cools the streams that, in the previous case, were cooled by the refrigeration cycles/heat pump, i.e. the branch of saline water from 10 °C to 3 °C and the heat generated in HGtS from the CO_2 dissolution in water and released in hydrate formation. The heat exchanger **E-4**, which integrated the heat of the CO_2 recycling stream after compression with the stream of water produced in the process, was removed. Considering there is no limitation on the amount of LNG used, the cooling of the CO_2 recycling stream is now done in **R-1**, reducing the number of heat exchangers required.

The outlet LNG temperatures were determined considering a $\Delta T_{min} =$ 5 °C, and the required LNG flow rate was determined. NG is obtained at the heat exchangers outlet as the LNG's phase change from liquid to gas occurs.

The heat to be provided for hydrate dissociation is supplied by a saline water stream that is fed at 10 °C and exits at 8 °C ($\Delta T_{min} = 5$ °C). As it is necessary to supply 2.8 MW_{th} and only the sensible heat of seawater is used, the mass flow rate needed is high (1247 $t{\cdot}h^{-1}$). It is considered that the saline water enters the process at 10 °C and 1 bar, and it is pressurised up to 1.5 bar to offset the pressure drop passing the dissociator. The inlet temperature of saline water as a hot utility in the dissociator can be increased, for example, by using solar panels, which reduces the flow rate required and, therefore, the electrical power of **P-5**. This is particularly pertinent in regions such as Sines, where temperatures of 40 °C are not uncommon during the summer season.

4.2. Economic evaluation

Regarding the equipment cost, the methodology followed for design and cost estimation is similar to that described for hydrate-based desalination using refrigeration cycles to generate cold utilities. Table 3 shows the cost per equipment and the main design specifications.

A total equipment cost of 2.5 M€ was estimated, which is 41 % lower than the case where refrigeration units were modelled. The cost decreased mainly due to the removal of the refrigeration cycle compressors. Still, the dissociator cost increased as seawater is used, increasing the flowrate and the area required to provide the heat for the dissociator, owing to the use of sensible instead of latent heat, thus the cost associated with the materials of construction of the exchanger. The equipment costs were updated from 2019 to 2023 using Eq. 3, resulting

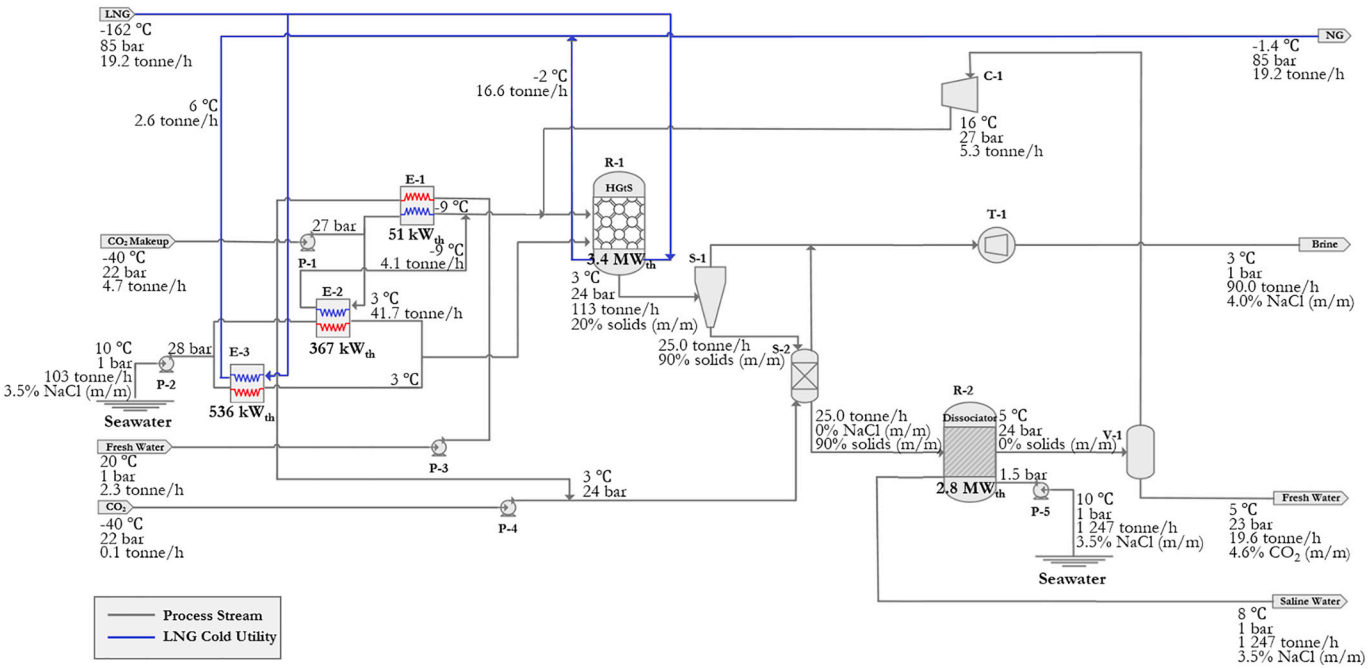

Fig. 7. – Hydrate-based desalination technology using CO_2 as hydrate-forming gas and LNG as a cold utility. Where *C* stands for compressor, *E* for heat exchanger, *P* for pump, *R* for reactor, *T* for turbine, *V* for flash vessel, *S* for separator and *VLV* for valve.

Table 3
– Equipment cost of hydrate-based desalination process using LNG as a cold utility.

	Total Cost/k€
CO_2 makeup pump (**P-1**)	34.9
Saline water pump (**P-2**)	249
Fresh water pump (**P-3**)	23.9
CO_2 pump (**P-4**)	19.3
Saline water (**P-5**)	423
CO_2/Fresh water heat exchanger (**E-1**)	0.78
CO_2/Saline water heat exchanger (**E-2**)	2.60
Saline water heat exchanger/LNG (**E-3**)	3.2
Brine turbine (**T-1**)	48.8
CO_2 compressor (**C-1**)	533
HGtS (**R-1**)	403
Dissociator (**R-2**)	532
Hydrocyclone (**S-1**)	98.2
Gas-Liquid separator (**V-1**)	146
Total	2516

in a $C_{equi}(2023€) = 3.3$ M€.

The CAPEX cost was calculated using Eq. 4 using the following values: $C_{equi}(2023€) = 3.3$ M€, $r_i = 0$, $\dot{P}_{FW} = 19.6$ t·h^{-1}, $N_{hours/year} = 8400$ h·yr^{-1} (2-week break per year), and $N_{years} = 25$ yr, which resulted in a CAPEX cost of 0.81 €·(tonne FW)$^{-1}$.

Concerning operating costs, the electrical power per equipment and the total electrical consumption of the process are shown in Table 4.

Table 4
– Electrical power in the hydrate-based desalination process using LNG as a cold utility.

	Electrical Power/ kW$_e$
CO_2 makeup pump (**P-1**)	0.66
Saline water pump (**P-2**)	93
Fresh water pump (**P-3**)	1.9
CO_2 pump (**P-4**)	6.5×10^{-3}
Saline water pump (**P-5**)	19
Brine turbine (**T-1**)	−50
CO_2 compressor (**C-1**)	10
Total	75

The total electrical power required for the hydrate-based desalination process using LNG cold utility is 75 kW$_e$, which results in an OPEX cost of 0.55 €·(tonne FW)$^{-1}$. The OPEX cost was reduced by 71 % concerning the base case where refrigeration cycles were modelled.

The total CAPEX and OPEX cost for the hydrate-based desalination process was estimated as 1.36 €·(tonne FW)$^{-1}$. This value is 57 % lower than the base case where refrigeration cycles were modelled.

The Specific Energy Consumption using LNG cold utility is 3.8 kWh·m^{-3}. The LNG cold utility places the SEC in the range of the values reported for RO (3–4 kWh·m^{-3} [14]). Thus, the hydrate-based technology using the regasification heat of LNG as cold utility makes this process competitive in terms of energy requirements, with the currently most used technology to desalinate seawater.

5. Conclusions

The seawater hydrate-based desalination process, using CO_2 as hydrate-forming gas and a HGtS as a hydrate-forming unit, was simulated in Aspen Plus. The process simulator introduced in this work enables the transfer of data from the lab scale to the industrial scale, boosting the development of hydrate-based processes. The ENRTL-RK model was chosen as the global property method to predict vapour-liquid and liquid-liquid equilibrium. This model demonstrated the closest prediction to the literature values of CO_2 solubility in salt water.

The process was modelled considering that 10 t·h^{-1} of CO_2 are fed to a HGtS unit, and the water treated has the seawater salt content. This enabled the production of 19.6 t·h^{-1} of fresh water.

For this production, two options of heat/cooling supply to the process have been evaluated. The first option considered the use of a refrigeration cycle/heat pump with ammonia as the cooling fluid; the second assessed the use of LNG as cold utility and seawater as hot utility.

For the case using a refrigeration cycle/heat pump, the total cost of producing fresh water was estimated at 3.29 €·(tonne FW)$^{-1}$, with CAPEX and OPEX costs of 1.38 and 1.92 € (tonne FW)$^{-1}$, respectively, and a SEC of 13.2 kWh·m^{-3}. The main costs of the process are associated with the ammonia refrigerant circuits that integrate the heat between the HGtS and dissociator and cool the feed streams. Replacing the

refrigeration cycles/heat pump with the LNG cold utility led to a total cost of 1.36 €·(tonne FW)$^{-1}$, with the CAPEX and OPEX costs of 0.81 and 0.55 € (tonne FW)$^{-1}$, respectively, and a SEC of 3.8 kWh·m^{-3}. This SEC of the seawater hydrate-based desalination process with LNG cold utility is competitive with RO (3–4 kWh·m^{-3}). Hence, this positions hydrate-based desalination technology as a cost-effective solution for addressing drinking water scarcity.

Author statement

Isabel S. Fernandes: Writing - Original Draft, Visualization, Software, Methodology, Investigation, Conceptualization. Mariana G. Domingos: Writing - Review & Editing, Validation, Formal analysis. Marcelo F. Costa: Validation, Formal analysis. Ricardo J. Santos: Writing - Review & Editing, Validation, Formal analysis, Supervision. José Carlos B. Lopes: Supervision, Formal analysis, Conceptualization.

Declaration of competing interest

The authors declare that they have no known competing financial interests or personal relationships that could have appeared to influence the work reported in this paper.

Acknowledgements

This work was financially supported by national funds through the FCT/MCTES (PIDDAC): (PIDDAC): LSRE-LCM, UIDB/50020/2020 (DOI: 10.54499/UIDB/50020/2020) and UIDP/50020/2020 (DOI: 10.54499/UIDP/50020/2020); and ALiCE, LA/P/0045/2020 (DOI: 10.54499/LA/P/0045/2020), and by the Portuguese Recovery and Resilience Plan (Next Generation EU): ATE - Alliance for Energy Transition (PRR - C644914747-00000023) and the funding program Interface Mission - Ref.: RE-C05-i02/2022 (call no. 01/C05-i02/2022 for Net4CO2 CoLAB and no. 03/C05-i02/2022 for STAR Institute CTI).

Appendix A. Supplementary data

Supplementary data to this article can be found online at https://doi.org/10.1016/j.desal.2024.118426.

Data availability

The authors are unable or have chosen not to specify which data has been used.

References

[1] Y. Ghalavand, M.S. Hatamipour, A. Rahimi, A review on energy consumption of desalination processes, Desalin. Water Treat. (2014) 1–16, https://doi.org/10.1080/19443994.2014.892837.
[2] J. Kucera, Desalination Water from Water, 1 ed, Wiley-Scrivener, 2014.
[3] S. Zhan, R. Yuan, Y. Huang, W. Zhang, B. Li, Z. Wang, J. Wang, Numerical simulation of hydrogen bubble growth and mass transfer on horizontal microelectrode surface under electrode-normal magnetic field, Phys. Fluids 34 (11) (2022), https://doi.org/10.1063/5.0127299.
[4] O. Oruc, I. Dincer, Assessing the potential of thermo-chemical water splitting cycles: a bridge towards clean and sustainable hydrogen generation, Fuel 286 (2021) 119325, https://doi.org/10.1016/j.fuel.2020.119325.
[5] A.D. Khawaji, I.K. Kutubkhanah, J.-M. Wie, Advances in seawater desalination technologies, Desalination 221 (1–3) (2008) 47–69, https://doi.org/10.1016/j.desal.2007.01.067.
[6] N. Ghaffour, T.M. Missimer, G.L. Amy, Technical review and evaluation of the economics of water desalination: current and future challenges for better water supply sustainability, Desalination 309 (2013) 197–207, https://doi.org/10.1016/j.desal.2012.10.015.
[7] P. Babu, A. Nambiar, T. He, I.A. Karimi, J.D. Lee, P. Englezos, P. Linga, A review of clathrate hydrate based desalination to strengthen energy–water nexus, ACS Sustain. Chem. Eng. 6 (7) (2018) 8093–8107, https://doi.org/10.1021/acssuschemeng.8b01616.
[8] S. Arnold, L. Wang, V. Presser, Dual-use of seawater batteries for energy storage and water Desalination, 18(43) (2022) 2107913. doi:https://doi.org/10.1002/smll.202107913.
[9] C. Delmas, Sodium and sodium-ion batteries: 50 Years of Research, 8(17) (2018) 1703137. doi:https://doi.org/10.1002/aenm.201703137.
[10] J.S. Sangwai, R.S. Patel, P. Mekala, D. Mech, M. Busch, Desalination of seawater using gas hydrate technology-current status and future direction, XVIII Conference on Hydraulics (2013) 4–6.
[11] A.B. Mhadeshwar, B.K. Peterson, M.S. Mettler, R.M. Billimoria, A. ExxonMobil Research and Engineering Company, NJ (US), Hydrates for water desalination using iso-butane additive, 2019.
[12] E.D. Sloan Jr, C.A. Koh, Clathrate Hydrates of Natural Gases, CRC press 2007.
[13] N.H. Duc, F. Chauvy, J.-M. Herri, CO2 capture by hydrate crystallization – a potential solution for gas emission of steelmaking industry, Energy Convers. Manag. 48 (4) (2007) 1313–1322, https://doi.org/10.1016/j.enconman.2006.09.024.
[14] Z.R. Chong, T. He, P. Babu, J.-n. Zheng, P. Linga, Economic evaluation of energy efficient hydrate based desalination utilizing cold energy from liquefied natural gas (LNG), Desalination 463 (2019) 69–80. doi:https://doi.org/10.1016/j.desal.2019.04.015.
[15] A. Parker, Potable water from sea-water, Nature 149 (3772) (1942) 184–186.
[16] T. He, S.K. Nair, P. Babu, P. Linga, I.A. Karimi, A novel conceptual design of hydrate based desalination (HyDesal) process by utilizing LNG cold energy, Appl. Energy 222 (2018) 13–24, https://doi.org/10.1016/j.apenergy.2018.04.006.
[17] K.-n. Park, S.Y. Hong, J.W. Lee, K.C. Kang, Y.C. Lee, M.-G. Ha, J.D. Lee, A new apparatus for seawater desalination by gas hydrate process and removal characteristics of dissolved minerals (Na+, Mg2+, Ca2+, K+, B3+), Desalination 274(1–3) (2011) 91–96. doi:https://doi.org/10.1016/j.desal.2011.01.084.
[18] R. Mccormack, A., J. Ripmeester, A., Clathrate desalination process using an Ultrasonic Actuator, 2013.
[19] Y. Seo, D. Moon, C. Lee, J.-W. Park, B.-S. Kim, G.-W. Lee, P. Dotel, J.-W. Lee, M. Cha, J.-H. Yoon, Equilibrium, kinetics, and spectroscopic studies of SF6 hydrate in NaCl electrolyte solution, Environ. Sci. Technol. 49 (10) (2015) 6045–6050, https://doi.org/10.1021/acs.est.5b00866.
[20] W.G. Knox, M. Hess, G. Jones, H. Smith, The hydrate process, Chem. Eng. Prog. 57 (2) (1961) 66–71.
[21] Y. Seol, J.-H. Cha, Increasing gas hydrate formation temperature for desalination of high salinity produced water with secondary guests, ACS Sustain. Chem. Eng. 1 (10) (2013) 1218–1224, https://doi.org/10.1021/sc400160u.
[22] A. Subramani, J.G. Jacangelo, Emerging desalination technologies for water treatment: a critical review, Water Res. 75 (2015) 164–187, https://doi.org/10.1016/j.watres.2015.02.032.
[23] R.A. McCormack, Clathrate Freeze Desalination Apparatus and Method, Ramco, Inc., 1996.
[24] J. Zhang, S. Chen, N. Mao, T. He, Progress and prospect of hydrate-based desalination technology, Front. Energy (2021) 1–15, https://doi.org/10.1007/s11708-021-0740-5.
[25] T. He, Z.R. Chong, J. Zheng, Y. Ju, P. Linga, LNG cold energy utilization: prospects and challenges, Energy 170 (2019) 557–568, https://doi.org/10.1016/j.energy.2018.12.170.
[26] P.E. Laranjeira, A.A. Martins, J.C.B. Lopes, M.M. Dias, NETmix®, a new type of static mixer: modeling, simulation, macromixing, and micromixing characterization, AICHE J. 55 (9) (2009) 2226–2243, https://doi.org/10.1002/aic.11815.
[27] P.E. Laranjeira, A.A. Martins, M.I. Nunes, J.C.B. Lopes, M.M. Dias, NETmix®, a new type of static mixer: experimental characterization and model validation, AICHE J. 57 (4) (2011) 1020–1032, https://doi.org/10.1002/aic.12316.
[28] J.C.B. Lopes, P.E.L. Laranjeira, M.M.Q. Dias, A.A. Martins, Network mixer and related mixing process, US 8434933 (2013).
[29] C.M. Fonte, M.E. Leblebici, M.M. Dias, J.C.B. Lopes, The NETmix reactor: pressure drop measurements and 3D CFD modeling, Chem. Eng. Res. Des. 91 (11) (2013) 2250–2258, https://doi.org/10.1016/j.cherd.2013.07.014.
[30] I.S. Fernandes, M.S.C.A. Brito, Y.A. Manrique, M.M. Dias, J.C.B. Lopes, R.J. Santos, Computational fluid dynamics model of two-phase flow in NETmix reactors, Chem. Eng. Technol. 44 (11) (2021) 2002–2010, https://doi.org/10.1002/ceat.202100245.
[31] I.S. Fernandes, M.S.C.A. Brito, Y.A. Manrique, M.M. Dias, J.C.B. Lopes, R.J. Santos, Experimental and numerical characterisation of two-phase flow in NETmix reactors, Chem. Eng. Process. Process Intensif. 109580 (2023), https://doi.org/10.1016/j.cep.2023.109580.
[32] M.F. Costa, C.M. Fonte, M.M. Dias, J.C.B. Lopes, Heat transfer performance of NETmix-A novel micro-meso structured mixer and reactor, AICHE J. 63 (6) (2017) 2496–2508, https://doi.org/10.1002/aic.15728.
[33] M.F. Costa, C.M. Teixeira, A.M. Lopes, J.P. Araújo, M.M. Dias, R.J. Santos, J.C.B. Lopes, Carbon capture and storage toward industrialization: a novel continuous process for the production of carbon dioxide clathrates, Energ. Technol. 10(6) (2022) 2100950. doi:https://doi.org/10.1002/ente.202100950.
[34] J.C.B. Lopes, M.M. Dias, M.F. Costa, R.J. Santos, C.M. Teixeira, Network heat exchanger device, method and uses thereof, 2018. US11484862B2.
[35] J.A.C.C. Santos, J.C.B. Lopes, F.G. Almeida, Closure plate for preloading a plate reactor, plate reactor and manufacturing method thereof. , PCT/IB2020/062568.
[36] Redes Energéticas Nacionais, The Natural Gas Sector, n.a. https://www.ren.pt/en-gb/activity/gas. (Accessed 22–02-11 2022).
[37] Global LNG Hub, Portugal facing gas supply constraints, 2021. https://globallnghub.com/portugal-facing-gas-supply-constraints.html. (Accessed 22–02-11 2022).
[38] J. Pospíšil, P. Charvát, O. Arsenyeva, L. Klimeš, M. Špiláček, J.J. Klemeš, Energy demand of liquefaction and regasification of natural gas and the potential of LNG for operative thermal energy storage, Renew. Sust. Energ. Rev. 99 (2019) 1–15, https://doi.org/10.1016/j.rser.2018.09.027.

[39] M.I. Khan, Comparative well-to-tank energy use and greenhouse gas assessment of natural gas as a transportation fuel in Pakistan, Energy Sustain. Dev. 43 (2018) 38–59, https://doi.org/10.1016/j.esd.2017.12.004.
[40] T. He, J. Zhang, N. Mao, P. Linga, Organic Rankine cycle integrated with hydrate-based desalination for a sustainable energy–water nexus system 291 (2021) 116839, https://doi.org/10.1016/j.apenergy.2021.116839.
[41] J. Park, J. Park, J. Kim, Process integration of light hydrocarbon separation and hydrate-based desalination for efficient and practical LNG cold energy recovery, Desalination 564 (2023) 116757, https://doi.org/10.1016/j.desal.2023.116757.
[42] J. Zheng, F. Cheng, Y. Li, X. Lü, M. Yang, Progress and trends in hydrate based desalination (HBD) technology: a review, Chin. J. Chem. Eng. 27 (9) (2019) 2037–2043, https://doi.org/10.1016/j.cjche.2019.02.017.
[43] C.-G. Xu, X.-S. Li, RSC Adv. 4 (2014), https://doi.org/10.1039/C4RA00611A.
[44] P. Babu, P. Linga, R. Kumar, P. Englezos, A review of the hydrate based gas separation (HBGS) process for carbon dioxide pre-combustion capture, Energy 85 (2015) 261–275, https://doi.org/10.1016/j.energy.2015.03.103.
[45] K.C. Kang, P. Linga, K.-n. Park, S.-J. Choi, J.D. Lee, Seawater desalination by gas hydrate process and removal characteristics of dissolved ions (Na+, K+, Mg2+, Ca2+, B3+, cl−, SO42−), Desalination 353 (2014) 84–90. doi:https://doi.org/10.1016/j.desal.2014.09.007.
[46] I.S. Fernandes, M.G. Domingos, M.F. Costa, R.J. Santos, J.C.B. Lopes, Preparation and pipeline transport of CO2 as a hydrate slurry – modelling and techno-economic analysis, Chem. Eng. Process. Process Intensif. 205 (2024), https://doi.org/10.1016/j.cep.2024.109973.
[47] S. Zeng, Z. Yin, J. Ren, D.R. Bhawangirkar, L. Huang, P. Linga, Effect of MgCl2 on CO2 sequestration as hydrates in marine environment: a thermodynamic and kinetic investigation with morphology insights, Energy 286 (2024) 129616, https://doi.org/10.1016/j.energy.2023.129616.
[48] J. Zhang, Y. Li, Z. Yin, P. Linga, T. He, X.Y. Zheng, Coupling amino acid L-Val with THF for superior hydrogen hydrate kinetics: implication for hydrate-based hydrogen storage, Chem. Eng. J. 467 (2023) 143459, https://doi.org/10.1016/j.cej.2023.143459.
[49] X. Liu, Y. Li, G.-J. Chen, D.-Y. Chen, B. Sun, Z. Yin, Coupling amino acid with THF for the synergistic promotion of CO2 hydrate Micro kinetics: implication for hydrate-based CO2 sequestration, ACS Sustain. Chem. Eng. 11 (15) (2023) 6057–6069, https://doi.org/10.1021/acssuschemeng.3c00593.
[50] S.M. Montazeri, N. Kalogerakis, G. Kolliopoulos, CO2 nanobubbles as a novel kinetic promoter in hydrate-based desalination, Desalination 574 (2024) 117296, https://doi.org/10.1016/j.desal.2024.117296.
[51] S.-C. Sun, C.-L. Liu, Y.-G. Ye, Phase equilibrium condition of marine carbon dioxide hydrate, J. Chem. Thermodyn. 57 (2013) 256–260, https://doi.org/10.1016/j.jct.2012.08.032.
[52] A.H. Mohammadi, W. Afzal, D. Richon, Gas hydrates of methane, ethane, propane, and carbon dioxide in the presence of single NaCl, KCl, and CaCl2 aqueous solutions: experimental measurements and predictions of dissociation conditions, J. Chem. Thermodyn. 40 (12) (2008) 1693–1697, https://doi.org/10.1016/j.jct.2008.06.015.
[53] P.D. Dholabhai, N. Kalogerakis, P.R. Bishnoi, Equilibrium conditions for carbon dioxide hydrate formation in aqueous electrolyte solutions, J. Chem. Eng. Data 38 (4) (1993) 650–654, https://doi.org/10.1021/je00012a045.
[54] A.L. Ballard, Non-ideal Hydrate Solid Solution Model for a Multi-Phase Equilibria Program, Colorado School of Mines, Arthur Lakes Library, 2002.
[55] G.K. Anderson, Enthalpy of dissociation and hydration number of carbon dioxide hydrate from the Clapeyron equation, J. Chem. Thermodyn. 35 (7) (2003) 1171–1183, https://doi.org/10.1016/s0021-9614(03)00093-4.
[56] R.F. Weiss, Carbon dioxide in water and seawater: the solubility of a non-ideal gas, Mar. Chem. 2 (3) (1974) 203–215, https://doi.org/10.1016/0304-4203(74)90015-2.
[57] Y.H. Li, T.F. Tsui, The solubility of CO2 in water and sea water, J. Geophys. Res. 76 (18) (1971) 4203–4207.
[58] C. Murray, J. Riley, The Solubility of Gases in Distilled Water and Sea Water—IV, Deep sea research and oceanographic abstracts, Elsevier, Carbon dioxide, 1971, pp. 533–541.
[59] C.-C. Chen, L.B. Evans, A local composition model for the excess Gibbs energy of aqueous electrolyte systems 32 (3) (1986) 444–454, https://doi.org/10.1002/aic.690320311.
[60] K. Udachin, C. Ratcliffe, J. Ripmeester, Structure, composition, and thermal expansion of CO2 hydrate from single crystal X-ray diffraction measurements, J. Phys. Chem. B 105 (2001), https://doi.org/10.1021/jp004389o.
[61] R.W. Henning, A.J. Schultz, V. Thieu, Y. Halpern, Neutron diffraction studies of CO2 clathrate hydrate: formation from deuterated ice, Chem. Eur. J. 104 (21) (2000) 5066–5071, https://doi.org/10.1021/jp0001642.
[62] S. Takeya, K.A. Udachin, I.L. Moudrakovski, R. Susilo, J.A. Ripmeester, Direct space methods for powder X-ray diffraction for guest−host materials: applications to cage occupancies and guest distributions in clathrate hydrates, J. Am. Chem. Soc. 132 (2) (2010) 524–531, https://doi.org/10.1021/ja905426e.
[63] Z. Duan, J. Hu, D. Li, S. Mao, Densities of the CO2–H2O and CO2–H2O–NaCl systems up to 647 K and 100 MPa, Energy Fuel 22 (3) (2008) 1666–1674, https://doi.org/10.1021/ef700666b.
[64] H. Teng, A. Yamasaki, Y. Shindo, Stability of the hydrate layer formed on the surface of a CO2 droplet in high-pressure, low-temperature water, Chem. Eng. Sci. 51 (22) (1996) 4979–4986, https://doi.org/10.1016/0009-2509(96)00358-2.
[65] Aspen Technology, Aspen Physical Property System, Physical Property Methods, Aspen Technology, Cambridge, MA, 2003.
[66] ASCO carbon dioxide Ltd, Vacuum insulated ASCO CO2 Storage Tanks, n.a. https://www.ascoco2.com/en/co2-and-dry-ice-equipment/co2-storage/vacuum-insulated-co2-and-crogyene-storage-tank. (Accessed 16 September 2020).
[67] D. Steen, Carbonated beverages, Chemistry and Technology of Soft Drinks and Fruit Juices (2016) 146–173, https://doi.org/10.1002/9781118634943.ch7.
[68] I.M. Abu-Reidah, Chapter 1 - carbonated beverages, in: C.M. Galanakis (Ed.), Trends in Non-alcoholic Beverages, Academic Press, 2020, pp. 1–36, https://doi.org/10.1016/B978-0-12-816938-4.00001-X.
[69] P.R. Ashurst, R. Hargitt, F. Palmer, Chapter 3 - ingredients in soft drinks, in: P. R. Ashurst, R. Hargitt, F. Palmer (Eds.), Soft Drink and Fruit Juice Problems Solved, Second edition, Woodhead Publishing, 2017, pp. 29–66, https://doi.org/10.1016/B978-0-08-100918-5.00003-5.
[70] P.D. Haney, Theoretical principles of aeration, J. Am. Water Works Assoc. 46 (4) (1954) 353–376.
[71] Q. Cui, S. Chandra, S. McCahan, The effect of dissolving gases or solids in water droplets boiling on a hot surface, J. Heat Transf. 123 (4) (2001) 719–728, https://doi.org/10.1115/1.1376394.
[72] D. Bhaumik, S. Majumdar, Q. Fan, K.K. Sirkar, Hollow fiber membrane degassing in ultrapure water and microbiocontamination, J. Membr. Sci. 235 (1) (2004) 31–41, https://doi.org/10.1016/j.memsci.2003.12.022.
[73] L.K. Wang, D.A. Vaccari, Y. Li, N.K., Shammas, chemical precipitation, in: L. K. Wang, Y.-T. Hung, N.K. Shammas (Eds.), Physicochemical Treatment Processes, Humana Press, Totowa, NJ, 2005, pp. 141–197, https://doi.org/10.1385/1-59259-820-x:141.
[74] J.R. Couper, W.R. Penney, J.R. Fair, S.M. Walas, Chemical Process Equipment: Selection and Design, Elsevier Inc., 2005.
[75] W.D. Seider, J.D. Seader, D.R. Lewin, Product & Process Design Principles: Synthesis, Analysis and Evaluation John Wiley & Sons, 2009.
[76] K. Xu, R. Smith, N. Zhang, Design and optimization of plate heat exchanger networks, in: A. Espuña, M. Graells, L. Puigjaner (Eds.), Computer Aided Chemical Engineering, Elsevier, 2017, pp. 1819–1824, https://doi.org/10.1016/B978-0-444-63965-3.50305-6.
[77] E. Commission, EU Blue Economy Observatory: Desalination, n.a. https://blue-economy-observatory.ec.europa.eu/eu-blue-economy-sectors/desalination_en. (Accessed 24–11-4 2024).
[78] M.K. Wittholz, B.K. O'Neill, C.B. Colby, D. Lewis, Estimating the cost of desalination plants using a cost database, Desalination 229 (1–3) (2008) 10–20, https://doi.org/10.1016/j.desal.2007.07.023.
[79] Eurostat, Electricity prices for non-household consumers - bi-annual data (from 2007 onwards), 2023. https://ec.europa.eu/eurostat/databrowser/view/nrg_pc_205/default/table?lang=en. (Accessed 10 June 2024).